Perfectly matched layers in the thin layer method

Citation: Barbosa, Joao Manuel de Oliveira, Joonsang Park, and Eduardo Kausel. "Perfectly Matched Layers in the Thin Layer Method." Computer Methods in Applied Mechanics and Engineering 217–220 (April 2012): 262–274.

As Published: http://dx.doi.org/10.1016/j.cma.2011.12.006

Publisher: Elsevier

Persistent URL: http://hdl.handle.net/1721.1/99347

Version: Author's final manuscript: final author's manuscript post peer review, without publisher's formatting or copy editing

Comput. Methods Appl. Mech. Engrg. 217-220 (2012) 262–274

Perfectly Matched Layers in the Thin Layer Method

by
João Manuel de Oliveira Barbosa[1]
Joonsang Park[2]
Eduardo Kausel[3]

Abstract

This paper explores the coupling of the *Perfectly Matched Layer* technique (PML) with the *Thin Layer Method* (TLM), the combination of which allows making highly efficient and accurate simulations of layered half-spaces of infinite depth subjected to arbitrary dynamic sources anywhere. It is shown that with an appropriate complex stretching of the thickness of the thin-layers, one can assemble a system of layers which fully absorbs and attenuates waves for any angle of propagation. An extensive set of numerical experiments show that the TLM+PML performance is clearly superior to that of a standard TLM model with paraxial boundaries augmented with buffer layers (TLM+PB). This finding strongly suggests that the proposed combination may in due time constitute the preferred choice for this class of problems.

Keywords: Perfectly Matched Layer Method; Thin-Layer Method; Elastodynamics; Soil-structure interaction; Green functions;

1. Introduction

The *Thin Layer Method* (TLM) is a semi-discrete numerical technique for the analysis of wave motion in layered media. It consists of a finite element discretization in the direction of layering combined with closed-form, analytical solutions for the remaining directions, along which the material properties are assumed to be constant. Alternatively, one can also analyze wave motion in one-dimensional waveguides of complicated cross-section —such as rails— by carrying out discretizations in not just one, but in two dimensions, and employing analytical solutions for the remaining third dimension [33], in which case the designation “thin-tube method” might be more appropriate. In general, the material layers can either be flat (i.e. horizontal layering)[17,41], or arranged into cylindrical [29] or spherical [30] layers. Fluid layers [12,26,36,39] and poroelastic layers [7] can also be considered. All of the previously cited problems belong to the more general class of *Partial Finite Elements* (PFEM), in which discretizations are carried out only within some arbitrary sub-space. This class encompasses also the finite cell method [40] in which the medium is discretized in the azimuthal and meridional directions while the radial direction is handled analytically. An analysis of the dispersion characteristics of the TLM is given in [31].

Since its inception in the early 1970’s [27,28,41], the TLM has found widespread use in soil dynamics and soil-structure interaction [37,38], non-destructive evaluation methods, seismic source simulations, wave propagation in waveguides of complex cross-section, wave propagation in laminated, anisotropic materials [20], waves in piezoelectric materials [8], heat diffusion in

[1] Doctoral Candidate, Department of Civil Engineering, University of Oporto, Portugal. Visiting student at MIT
[2] Senior Geophysicist, Norwegian Geotechnical Institute, Oslo, Norway
[3] Professor of Civil and Environmental Engineering, Massachusetts Institute of Technology, Cambridge, MA 02139

layered composites [15], consolidation in poroelastic media, solid-fluid interaction [39], and in many more areas of application. Although the origin and early development of the TLM technique hark back to the early 1970's, the designation TLM became common only since the beginning of the 1990's. Initially, the TLM was limited to bounded domains such as layers underlain by rigid base (i.e. rock) but soon *Paraxial Boundaries* (PB) became available which allowed the simulation of infinite domains [14,34,35]. A brief historical account is given in [30].

On the other hand, the *Perfectly Matched Layer* (PML) is a numerical technique used for purposes similar to those of absorbing or transmitting boundaries, namely to suppress undesirable echoes and reflections of waves in infinite media modeled with discrete, finite systems. It is based on stretching the space by means of position-dependent, complex-valued scaling functions which begin with unit values at the interface or horizon delimiting the elastic region. The stretching functions then attain progressively larger complex values with distance from this horizon, which causes the waves within the PML to attenuate exponentially [16]. It can also be shown that the impedance contrast at the PML boundary is unity, in which case no reflections take place no matter what the angle of propagation of the waves entering the PML region should be.

The PML concept made its debut in the 1990's [4] and because of its excellent performance found rapid adoption in engineering science, especially for electromagnetic wave propagation models cast with finite differences. In more recent years, the PML has also been used widely for problems of elastic wave propagation in both structural mechanics and in geophysics [3,9,10,13,42]. A good literature review on the subject can be found in [25].

Technical publications examining various theoretical and mathematical aspects of PMLs also abound. Of special relevance and interest to the material herein is a series of papers on the spectral properties of PMLs [5,6,11,32], which explore the characteristics of the eigenvalues of continuous PMLs —i.e. without discretization errors— in the context of electromagnetic waves in the frequency domain. It can be shown that the eigenvalues alluded to in those papers are closely related to the modes of propagation of SH (i.e. Love) waves in a layer underlain by an elastic half-space, and thus some of the findings therein are relevant to the TLM, as will be seen.

In the ensuing we apply the perfectly matched layer concept to the thin-layer method. To keep matters simple, we begin with a homogeneous stratum of complex thickness subjected to out-of-plane (i.e. anti-plane or SH) loads, define its transformation into a PML, overlay an elastic layer on top, and finally examine the characteristics and efficiency of the combination in the context of the TLM technique. We then go on exploring the more complicated case of SVP waves whose characteristics depend also on Poisson ratio. Finally, we compare the performance of the TLM+PML against that of the TLM+PB based on conventional paraxial boundaries.

2. Continuous PML for SH waves

Consider a homogeneous, elastic stratum of total depth H subjected to SH waves which propagate with celerity C_S. Following the usual strategy, we convert this stratum into a PML by transforming the vertical coordinate z into its complex, stretched counterpart $\overline{z}$ written as

$$\overline{z} = z - \mathrm{i}\,\Psi(z) \tag{1}$$

where $\Psi(z)$ is a function yet to be defined. The usual choice for $\Psi(z)$ guaranteeing evanescence of waves within the PML is

$$\Psi(z)=\int_0^z \psi(s)\,ds \qquad\qquad 0\le z\le H \tag{2}$$

in which $\psi(s)>0$ is an always positive *stretching* function. In principle the shape of $\psi(s)$ is arbitrary as long as it is continuous and $\Psi(0)<\Psi(H)$ [6]. However, once the domain is discretized into thin layers —or for that matter, into finite elements— spurious reflections take place due to the abrupt, even if small, changes in $\psi(z)$, so it behooves for this function to increase smoothly with *z*. A commonly used stretching function $\psi(z)$ is [10]

$$\psi(z)=\frac{\omega_o}{\omega}\left(\frac{z}{H}\right)^m \tag{3}$$

where ω_o controls the degree of absorption of the wave and $m>0$ defines the rate of stretching within the PML. This implies

$$\Psi(z)=\frac{\omega_o H}{\omega(m+1)}\left(\frac{z}{H}\right)^{m+1} \tag{4}$$

which can be written compactly as

$$\Psi(z)=\Omega H\zeta^{m+1} \tag{5a}$$

where

$$\Omega=\frac{\omega_0}{\omega(m+1)}, \qquad\qquad \zeta=\frac{z}{H} \tag{5b}$$

The stretched vertical coordinate then simplifies to

$$\bar{z}=z\left(1-\mathrm{i}\Omega\zeta^m\right) \tag{6}$$

which implies a total complex depth $\bar{H}=H\left[1-\mathrm{i}\Omega\right]$.

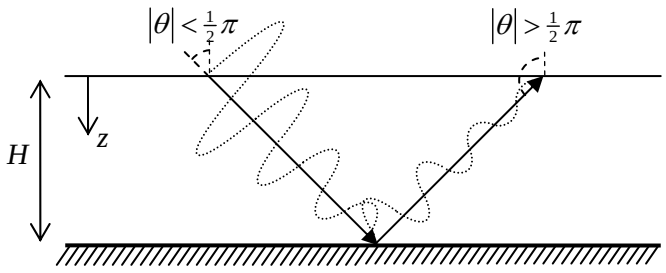

Figure 1 – Propagation of wave in the PML region

Consider now a plane SH wave traveling at an angle θ with respect to the vertical direction z, which we assume here to be positive downwards and starting from the free surface (Fig. 1). In stretched space, this wave can be expressed as

$$\begin{aligned} u(x,\bar{z},t) &= A\,\mathrm{e}^{\mathrm{i}\left(\omega t - x\frac{\omega}{C_S}\sin\theta - \bar{z}\frac{\omega}{C_S}\cos\theta\right)} \\ &= A\,\mathrm{e}^{\mathrm{i}\left(\omega t - x\frac{\omega}{C_S}\sin\theta - z\frac{\omega}{C_S}\cos\theta\right)}\,\mathrm{e}^{-\frac{\omega}{C_S}\cos\theta\,\Psi(z)} \end{aligned} \tag{7}$$

Inasmuch as (5a) guarantees $\Psi(z)>0$ to increase monotonically and smoothly with z, and the other parameters are positive i.e. $\omega>0$ and $-\frac{1}{2}\pi<\theta<\frac{1}{2}\pi$ (i.e. $\cos\theta>0$), this expression represents an evanescent wave which decays exponentially as it propagates down. Clearly, this very same rule guarantees also that the small reflection from the bottom boundary will decay upwards, because in that case $|\theta|>\frac{1}{2}\pi$ and $\cos\theta<0$. Now, a plane SH wave which enters the PML with an amplitude A reaches the rigid base at the bottom, $z=H$, with an amplitude $A\exp\left(-\omega\cos\theta\,\Psi(H)/C_S\right)=A\exp\left(-\omega\cos\theta\,\Omega H/C_S\right)$. In the light of eq. 5b, this implies in turn that the total downward attenuation equals $A\exp\left(-\omega_0\cos\theta\,H/C_S/(m+1)\right)$ which for fixed values of $\omega_0 H$ is independent of frequency. On the other hand, equation 5a shows that the total stretching is controlled by the factor ΩH, and as long as this product is inversely proportional to frequency, then the total downward attenuation will remain constant. Clearly, this goal can be accomplished just as well by choosing Ω to be constant and taking the depth H of the PML to be inversely proportional to the frequency, i.e. proportional to the characteristic wavelength, as done in the ensuing. Now, since $C_S=\omega\lambda/2\pi$, with λ being the wave length, the wave reaches the base with an amplitude $A\exp\left(-2\pi\cos\theta\,\Omega H/\lambda\right)$. This wave elicits in turn a reflection which emerges back at the surface with an amplitude equal to the square of the previous one, i.e. $A\exp\left(-4\pi\cos\theta\,\Omega H/\lambda\right)$. Hence, the total roundtrip decay Δ of the wave is then

$$\Delta = \mathrm{e}^{-4\pi\Omega\,\eta\cos\theta} \tag{8}$$

where

$$\eta = H/\lambda \tag{9}$$

Clearly, as long as the thickness of the layer is made proportional to the wavelength (i.e. η is chosen as a constant), the effectiveness of the PML as measured by eq. (8) for any given angle of incidence depends solely on the dimensionless parameter Ω. On the other hand, a ray entering the PML at x_0 with an inclination θ returns to the surface at a distance $r=x-x_0=2H\tan\theta$ from the point of penetration, i.e.

$$\frac{r}{\lambda} = 2\eta\tan\theta \tag{10}$$

Equations (8-10) indicate that the higher the horizontal range of interest is, the higher the value needed for Ω, η, or both.

We now examine the effectiveness of this medium as a PML. For this purpose, consider an elastic half-space with shear modulus $G = 1$ [Pa] and shear wave velocity $C_S = 1$ [m/s] excited by an SH line source acting at a depth z_s with frequency $\omega = 2\pi$ [rad/s]. For an elastic medium, the exact solution for the displacement observed at a receiver at range x and depth z_r is (e.g. see [23, p. 69]):

$$u = \frac{1}{4\mathrm{i}G}\left[H_0^{(2)}(kr_1) + H_0^{(2)}(kr_2)\right], \qquad k = \frac{\omega}{C_S} = \frac{2\pi}{\lambda}, \qquad r_{1,2} = \sqrt{x^2 + (z_s \mp z_r)^2} \qquad (11)$$

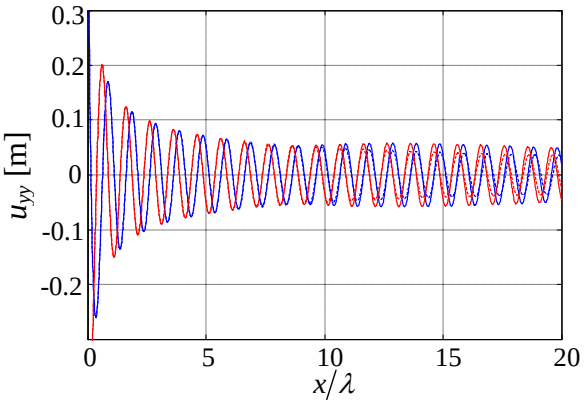

Figure 2 – Real (blue) and imaginary (red) parts of displacements at the surface of half-space: Dashed line = PML approximation; Solid line = exact solution (differences virtually nil)

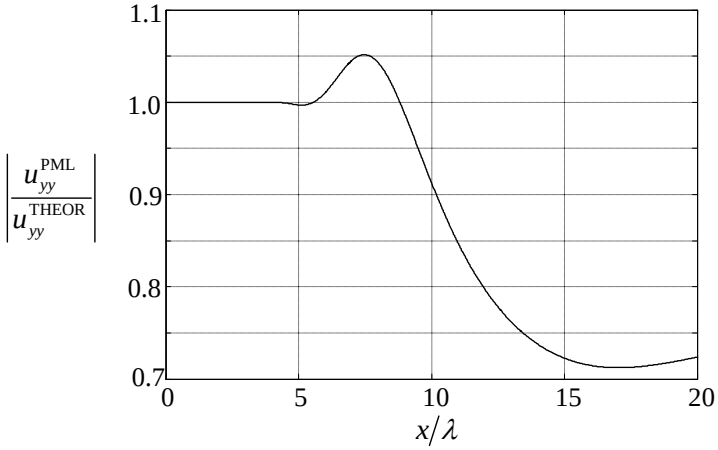

Figure 3 – Ratio of displacements at surface of the PML and those of the half-space

By contrast, the PML admits an exact solution based on an expansion in terms of the normal modes of the stratum, as given by e.g. [23, p. 130], and accounting for the fact that the vertical dimensions have been stretched:

$$u_{yy}(x,\omega)=\frac{1}{\mathrm{i}G}\sum_{j=1}^{\infty}\phi_j(\overline{z}_s)\phi_j(\overline{z}_r)\frac{\mathrm{e}^{-\mathrm{i}k_j|x|}}{k_j\overline{H}} \tag{12a}$$

$$k_j=\sqrt{\left(\frac{\omega}{C_S}\right)^2-\left(\frac{\pi(2j-1)}{2\overline{H}}\right)^2}\quad,\qquad \mathrm{Im}\,k_j<0 \tag{12b}$$

$$\phi_j(\overline{z})=\cos\left(\frac{\pi(2j-1)}{2}\frac{\overline{z}}{\overline{H}}\right) \tag{12c}$$

where $\overline{z}_s$ and $\overline{z}_r$ are the stretched depths of the source and of the receiver, respectively, and $\overline{H}$ is the total stretched depth. With $\lambda=C_s/f=1$ [m], and choosing for the PML the parameters $\eta=H/\lambda=\frac{1}{2}$, $H=\frac{1}{2}$ [m], a maximum range $r\le x_{\max}=5\lambda=5$ [m], a roundtrip decay of two orders of magnitude i.e. $\Delta=10^{-2}$, and $m=2$, we infer

$$\tan\theta_{\max}=\frac{x_{\max}}{2\eta\lambda}=\frac{5}{2\times\frac{1}{2}}=5\qquad\Rightarrow\theta_{\max}=78.7^\circ\qquad\Rightarrow\qquad\cos\theta_{\max}=0.196\,, \tag{13a}$$

$$\Omega=\frac{\ln\Delta^{-1}}{4\pi\eta\cos\theta_{\max}}=\frac{\ln 100}{4\pi\frac{1}{2}\times 0.196}=3.74 \tag{13b}$$

$$\overline{H}=H-\mathrm{i}\Psi(H)=H[1-\mathrm{i}\Omega]=0.5\times[1-3.74\mathrm{i}]=0.5-1.87\mathrm{i} \tag{13c}$$

Using these data, we construct a PML, subject it to an SH line source at its surface $\overline{z}_s=0$, and compute the displacements for receivers at variable range on the surface $\overline{z}_r=0$ by means of eq. (12a). Fig. 2 compares the displacements thus computed against the displacements on the surface of the half-space predicted by eq. (11). As can be seen, both the real and imaginary parts of the displacements agree perfectly until a range of about $x=8\lambda$ is exceeded. On the other hand, Fig. 3 shows the ratio between the absolute values of the maximum displacements at each range obtained by the two approaches. This figure confirms that until the distance $x_{\max}=5\lambda$, the ratio of amplitudes is virtually one, with an error less than 1%. Then again, at the distance $x=8\lambda$ the error has grown to approximately 5%, and thereafter it increases substantially. This shows that with the chosen parameters and as seen from its surface, the PML behaves essentially as an elastic half-space, yet is a perfect absorber of waves only up to some maximum range which depends on the parameters chosen.

The above results notwithstanding it should be noted that the closed-form modal solution herein relied upon for comparison with the half-space suffers from at least one *Schönheitsfehler* i.e. from a “beauty imperfection”. It has to do with the fact that for interior points, the ratio $\overline{z}/\overline{H}$ remains complex namely

$$\frac{\overline{z}}{\overline{H}}=\zeta\frac{1-\mathrm{i}\Omega\zeta^m}{1-\mathrm{i}\Omega}=\frac{\zeta}{1+\Omega^2}\left[1+\Omega^2\zeta^m+\mathrm{i}\Omega\left(1-\zeta^m\right)\right]$$

Thus, when this ratio is substituted into (12c), either for a source or for a receiver within the PML, the expansion of the cosine function will result in hyperbolic terms which grow and oscillate wildly at depth, both of which produce severe cancellation errors and may even cause the series to fail to converge altogether, as shown in the Appendix. Thus, the modal expansion, although formally correct, breaks down for points within the PML. It can thus be expected that similar problems might arise in the TLM version of the PML, and that is partly the case, at least within the PML part (see the Appendix).

3. PML for SH waves via the TLM

We now proceed to construct a PML by means of a stack of thin layers in the context of the TLM. As shown in an earlier paper by the writers [24], a very simple way to construct a PML with finite elements is to directly stretch the elements' linear dimensions in accord with their horizontal and vertical position within the PML. In the TLM, this recipe translates into replacing the thicknesses of the thin layers composing a PML with their complex counterparts, which depend in turn on the location (i.e. depth) of the thin layers within the PML. Thus, if we assume that the PML is divided into N equal layers, then the stretched thickness $\overline{h}_\ell$ of the ℓ^{th} thin-layer is

$$\overline{h}_l = \overline{z}_\ell - \overline{z}_{\ell-1} = H\left\{\frac{1}{N} - \mathrm{i}\,\Omega\left[\left(\frac{\ell}{N}\right)^{m+1} - \left(\frac{\ell-1}{N}\right)^{m+1}\right]\right\} \tag{14}$$

which assumes that $1 \le \ell \le N$ with ℓ increasing downwards. On the other hand, in the TLM, each of the thin layers is characterized by elementary layer matrices $\mathbf{A}_\ell, \mathbf{G}_\ell, \mathbf{M}_\ell$ [17,19], two of which are proportional to the sub-layer thickness, while the remaining one is inversely proportional to that thickness, i.e.

$$\mathbf{A}_\ell = h_\ell\left[\cdot\,\cdot\right]; \qquad \mathbf{G}_\ell = h_\ell^{-1}\left[\cdot\,\cdot\right]; \qquad \mathbf{M}_\ell = h_\ell\left[\cdot\,\cdot\right] \tag{15}$$

The matrix elements contained within the brackets, which depend on the material properties and the interpolation order being used, can be found in earlier articles on the TLM, although they are not actually needed in the context of this article. The important point here is that they depend in some fashion on the sub-layer thickness h_ℓ, either as multiplicand or as divisor. To obtain the layer matrices for the PML, it suffices then to substitute $\overline{h}_\ell$ in lieu of h_ℓ. Thereafter, the layer matrices are overlapped as usual, which leads us to the block-tridiagonal system matrices $\mathbf{A} = \{\mathbf{A}_\ell\}$, $\mathbf{G} = \{\mathbf{G}_\ell\}$, $\mathbf{M} = \{\mathbf{M}_\ell\}$. In the TLM, these are then used to formulate the linear eigenvalue problem in the horizontal wavenumber squared k_j^2 for SH waves

$$\left(\mathbf{A}k_j^2 + \mathbf{G} - \omega^2\mathbf{M}\right)\boldsymbol{\phi}_j = \mathbf{0} \tag{16}$$

with ω being the frequency and $k_j, \boldsymbol{\phi}_j$ the eigenvalues and modal shapes, respectively. In the classical TLM formulation, these modes satisfy the orthogonality conditions [41]

$$\boldsymbol{\phi}_i^T\ \mathbf{A}\,\boldsymbol{\phi}_j = k_j\delta_{ij}\,, \qquad \boldsymbol{\phi}_i^T\left(\mathbf{G} - \omega^2\mathbf{M}\right)\boldsymbol{\phi}_j = -k_j^3\delta_{ij} \tag{17}$$

where δ_{ij} is the Kronecker delta. In the case of a PML composed of N thin layers and when using a linear expansion, the eigenvalue problem yields $2N$ eigenvalues $\pm k_j, \boldsymbol{\phi}_j$, half of which satisfy the condition $\mathrm{Im}\, k_j \le 0$, and the other half satisfy $\mathrm{Im}\, k_j \ge 0$, which we discard because they represent waves that grow with x. The displacements in the PML due to an SH line load (i.e. the anti-plane Green's function) are now obtained from the modal combination [17]

$$u_{yy}(x) = \frac{1}{2i} \sum_{j=1}^{N} \phi_j^s \phi_j^r \frac{e^{-i k_j |x|}}{k_j} \tag{18}$$

where ϕ_j^s and ϕ_j^r are the *normalized* components of the j^{th} eigenmode at the elevation of the source and of the receiver, respectively, and the sign of k_j is chosen so that $\mathrm{Im}\, k_j < 0$.

We now choose a PML divided into $N = 20$ linear thin-layers, i.e. 40 thin-layers per wave-length (which is more than enough), solve the eigenvalue problem (16) using Matlab, and compute the displacements via (18). Fig. 4 shows the ratio of the absolute value of the displacements predicted by (18) and the absolute value of the displacements of a half-space given by (11).

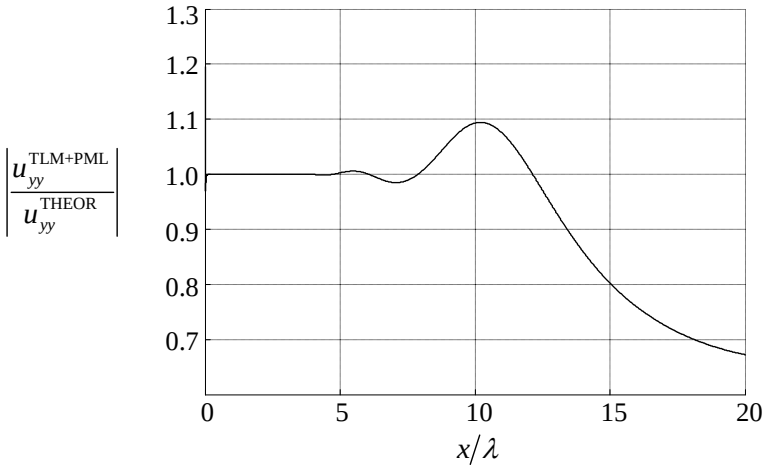

Figure 4 – Ratio: TLM+PML / Half-space

Comparing Fig. 4 with Fig. 3 we observe that the results are rather similar, including the maximum horizontal distance (i.e. range $x_{\max} = 5\lambda$) to which the error is negligible. However, we also observe that at very small distances from the source a dip can be discerned where the discrete TLM solution begins to deviate from the exact solution. The reason is, of course, that in the exact solution, the displacement at the location of the source is singular, whereas in the discrete solution, it remains finite. Although this could be remedied by increasing the refinement of the model, this is usually unnecessary, especially if distributed sources without singularities are considered, in which case the above small deviation is wholly inconsequential. Additional considerations on convergence are given in the Appendix.

An extensive series of numerical experiments and regression analyses (not shown) suggest that optimal choices for the parameters of the PML are

$$m = 2\,, \qquad \eta = \frac{H}{\lambda} = \sqrt[3]{\tfrac{1}{12} x_{\max} / \lambda} \geq 1\,, \qquad nN = 10\eta\,, \qquad \Omega = 4\eta \tag{19}$$

where N is the number of thin layers in the PML and n is the expansion order used in the discretization (usually $n = 1$ or $n = 2$). For example, $\eta = 10$, $\Omega = 40$, $n = 1$ and $N = 100$ would allow obtaining results on the surface of the PML with errors less than 0.5 % up to ranges as large as $x_{\max} = 12{,}000\lambda$ (yes, an astonishing four orders of magnitude!), as illustrated in Fig. 5. We may add that the PML considered herein has no material damping of any kind.

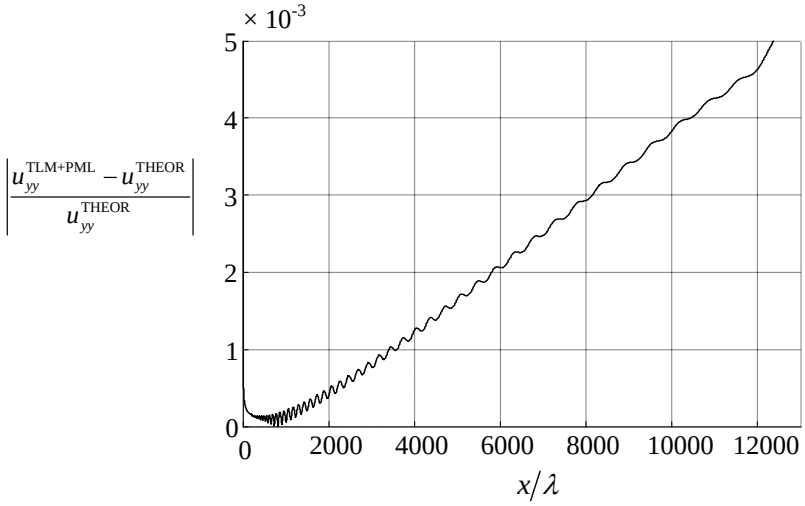

Figure 5 – Relative error as function of horizontal range

Finally, we mention in closing that as in the continuous case, the discrete modes attain large, oscillatory amplitudes within the PML which lead to severe cancellation errors when one attempts to determine displacements for $z_r > 0$ and/or for a source within the PML, $z_s > 0$. However, in general such computations are not necessary, provided the PML behaves as expected when seen from its surface. In other words, what matters here is the absorption capacity of the PML, not the response within that device (see also the Appendix).

4. Unphysical modes of PML+elastic layer

In the previous section, it was shown that a PML consisting of uniform thin layers with complex thickness behaves —at least as seen from it upper surface— like an elastic half-space. Furthermore, the comparison with the half-space was assessed by means of a modal superposition with the normal modes of the PML given from the solution of the eigenvalue problem (eq. 16). It could thus be expected that if the PML were overlain by an elastic layer and the solution again found by modal superposition with modes obtained via the TLM, one would obtain within the elastic layer a solution which is nearly indistinguishable from that of a layer on an elastic half-space. Although this is largely true, it behooves first to elaborate on some subtle complications. To elucidate the nature of these, consider a uniform layer underlain by an elastic

half-space with impedance higher than that of the layer, a combination which defines the well-known wave guide for Love waves. Also, the system contains an SH source at some arbitrary location in the upper elastic layer.

When the exact, continuous solution is formulated for this problem, the classical approach is to assume a displacement ansatz in the half-space which only contains waves that satisfy the radiation and boundedness conditions at an infinite depth, a formulation which leads to the *normal modes* of the layered medium. However, it is also possible to find solutions —the *leaky waves* or unphysical modes— which violate such conditions [1,2]. Mathematically, these correspond to the poles of the characteristic, transcendental equation for Love waves obtained in the so-called *lower Riemann sheet* whose modes grow exponentially with depth, which implies that they contain an infinite energy and do not satisfy orthogonality conditions —at least in the case of a continuum— which is also why they are sometimes referred to as the "forbidden" modes. In principle, when the solution is worked out by hand, one uses only the normal modes which satisfy the conditions at infinity, but then again because the medium is infinitely deep, the modal set is incomplete, in which case one must add additional terms referred to as *branch cut integrals*, which represent body waves radiating into the half-space.

In the TLM, however, one discretizes both the elastic layer and the PML into sub-layers which are thin in the finite element sense and finds the modes of that combination from the solution to the eigenvalue problem (eq. 16). It will then be found that the modal set above will contain a combination of *both* the physical and unphysical modes [5,6,11] which —very roughly speaking— arise because the lower horizon in the PML represents "infinity" in the half-space. In addition, a new set of purely mathematical modes appear, namely the so-called *Bérenger modes*. As it turns out, the contributions to the response of both the leaky and Bérenger modes make up for the loss (or absence) of branch integrals in the TLM, and the modal set is once more complete, and in that sense, such modes are indeed welcome. These modes will be revisited in more detail in a later section.

Unfortunately, the presence of the modes of rapid —even if finite— growth within the PML substrate may break down the solution to the eigenvalue problem, especially with refined models composed of many thin layers. Indeed, as the refinement of the model is increased and more sub-layers are added, the higher the risk that modes may appear which fail the orthogonality conditions, although this is relatively rare. Still, since the quadratic eigenvalue problem in the TLM is usually solved either via inverse iteration with shift by the Rayleigh quotient or by a determinant search with deflation of the eigenvalues already found, and thus the eigenvalues and eigenvectors are extracted one at a time, it is possible to test the modes as they are being found and enforce orthogonality as needed to prevent a numerical breakdown. Similar strategies apply also to the more complicated in-plane case involving SVP waves treated later on. Admittedly, in the examples worked out in the ensuing we have bypassed these difficulties and used Matlab's convenient routine **eig**, which does not rely on orthogonality conditions to extract the eigenvalues, and thus is not affected to the same degree by the numerical problems previously alluded to. However, the eigenvectors thus found must still be verified and re-orthogonalized individually as may be needed, a step which makes a big difference in the success of the method (an economic strategy is to enforce orthogonality with respect to the sum of the previously found eigenvectors). The heavy price paid, however, is that Matlab neither takes advantage of the

block-tridiagonal, narrowly banded nature of the matrices, nor offers a direct solution to the quadratic eigenvalue problem for SVP waves. Hence, the latter must be expressed as a linear eigenvalue problem of double dimension involving non-symmetric, non-sparse matrices. Thus, the use of Matlab in the context of large models is highly inefficient, both computationally and also because of the memory required to store the large matrices. Still, the quadratic eigenvalue solver is a distinct issue from the subject at hand, which shall be the subject of a separate companion paper by the writers.

5. Elastic half-space as combination of elastic layer & PML

We now proceed to model once more a homogeneous elastic half-space, but this time by overlying the PML with an elastic layer of the same properties as the half-space. The purpose is to assess the quality of the TLM response within the half-space by comparison with the analytical solution (i.e. yardstick or canonical problem) given by eq. 11. By contrast, if we were to deal with a half-space overlain with either a softer or stiffer layer, we would lack such convenient yardstick for verification, even for SH waves.

Consider then an elastic layer with shear wave velocity $C_S = 1$ [m/s] and mass density $\rho = 1$ [kg/m^3], which is underlain by an elastic half-space of the same properties, but modeled as a PML. Neither the layer nor the half-space has any damping. Using a linear expansion $n = 1$, the layer has a total thickness $H_1 = 6\lambda$ divided into $N_1 = 120$ thin layers, while for the PML, we choose parameters satisfying the optimality criteria given earlier for accurate results up to a distance $x_{\max} = 20\lambda$. These parameters work out to be $m = 2$, $\eta = 2.4$, $\Omega = 8.67$, $H_2 = 2.4\lambda$, and $N_2 = 24$. Thus, the TLM model has a total of 144 thin layers. Also, we subject this model to an SH line source at $x = 0$, $z = 6\lambda$, that is, placed at the interface of the elastic layer and the PML. Although displacements can be computed anywhere within the elastic layer, we chose herein to evaluate these at the same elevation as the load. Fig. 6 shows a comparison of the TLM+PML solution against the exact formula as function of the horizontal distance, and the results are just splendid, for they match to a degree that can't be distinguished at the scale of the drawing. Thus, we have verified that the combination TLM+PML works very well indeed, at least for SH waves.

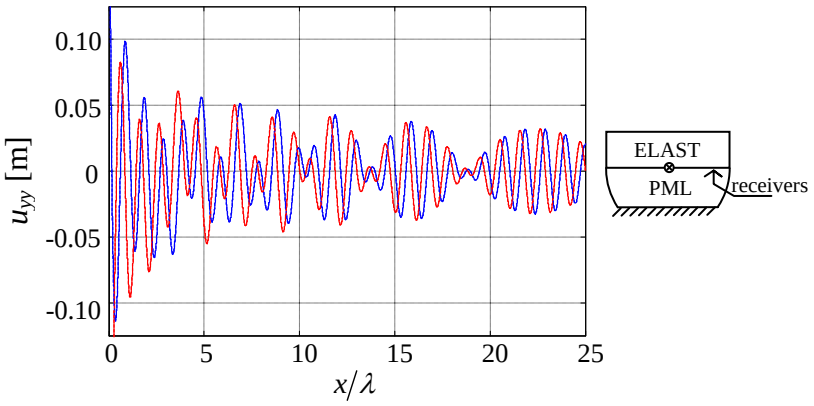

Figure 6– Real (blue) and imaginary (red) parts of displacements within half-space: Dashed and solid lines are the PML approximation and exact solutions, respectively. Differences are undetectable, even at a larger scale.

6. Love waveguide subjected to an SH source

Next, we go on to apply the technique described to a soft layer underlain by a stiffer half-space, i.e. a Love waveguide, and subject it to an SH source of varying frequency f applied again at the interface of the layer and the half-space, which have shear wave velocity C_{Sj}, mass density ρ_j, material damping ξ_j, and total thickness H_j, with $j=1,2$. The properties chosen are:

Layer: $C_{S1}=0.5$ [m/s], $\rho_1=1$ [kg/m^3], $\xi_1=0.005$, $H_1=1$ [m], $N_1=200$

PML: $C_{S2}=1$ [m/s], $\rho_2=1$ [kg/m^3], $\xi_2=0.005$, $\eta=2$, $\Omega=6.67$, $H_2=\eta\lambda=2\lambda=2/f$ [m], $N_2=20$

The optimal parameters are chosen using the highest frequency, i.e. the shortest wavelength, just to keep matters simple. Nonetheless, the PML's total thickness changes with the frequency in such way that the smaller the frequency, the thicker the layers in the PML. We subject this system to the four frequencies $f=\{0.1, 0.2, 1, 10\}$ [Hz].

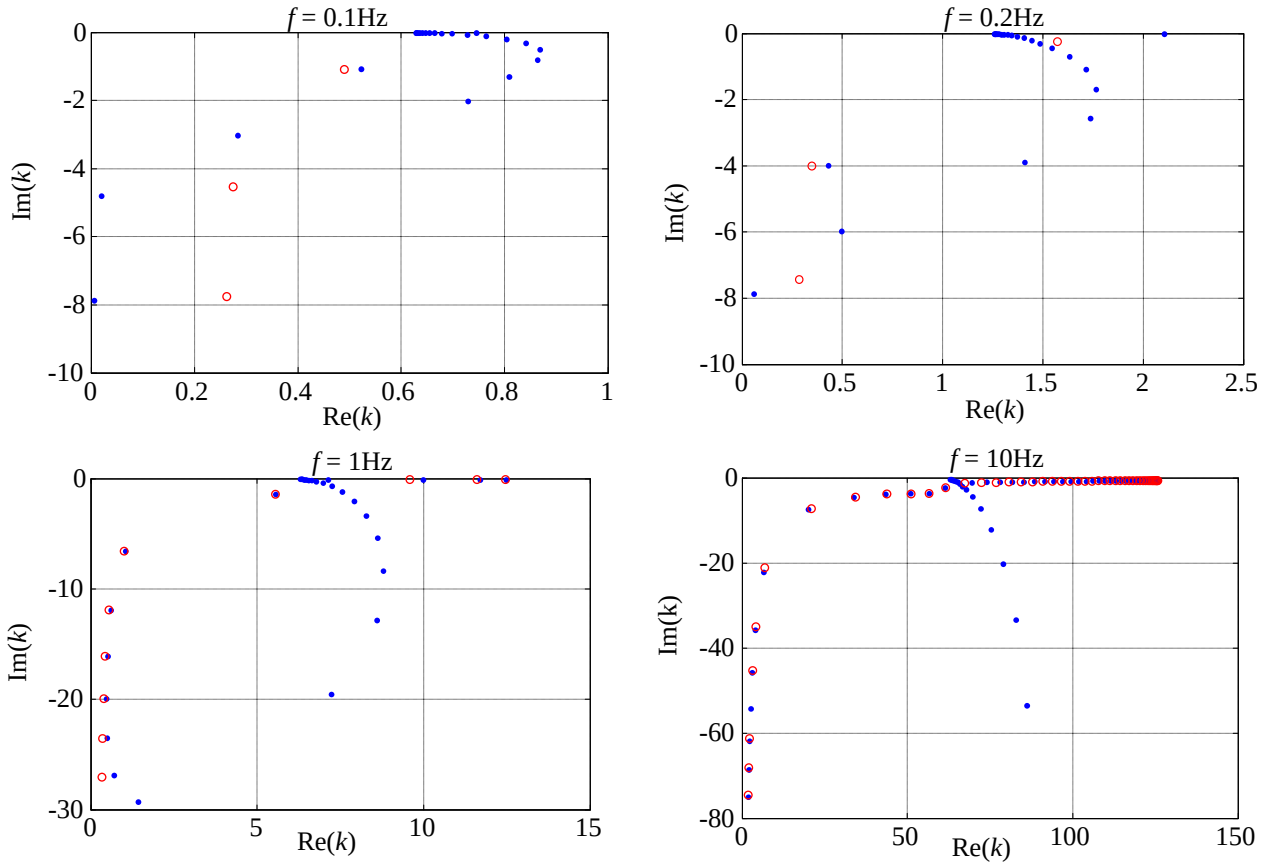

Figure7 a,b,c,d: Poles of the Love waveguide at four different frequencies. Blue dots are the TLM solution while red circles are the analytical solution obtained via search techniques.

Figures 7a-d show a comparison of the normal modes (i.e. poles) obtained with the TLM as solid blue dots, while an analytical solution based on search techniques shows these poles as hollow red circles. Both the physical as well as the unphysical modes are included. A very striking feature in the map of poles is the presence of the curved, dense line of poles on the right, which

are referred to as the Bérenger modes. We mention also that although at low frequencies the numerical and analytical sets of poles may not seem to be close to each other —even if their agreement improves with frequency— nonetheless the displacements are stupendously accurate for all four frequencies.

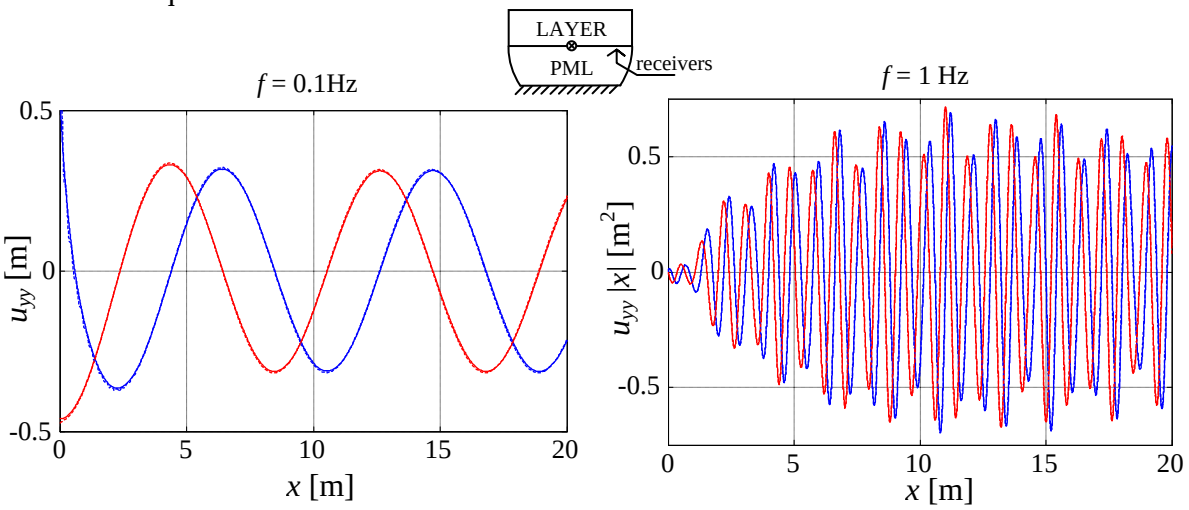

Figure 8 a,b: Real (blue) and imaginary (red) parts of displacements u_{yy} in a Love waveguide due to an SH line load placed at the interface of the layer and the half-space. Solid line = TLM+PML model; Dashed line = numerical integration. Differences are undetectable.

Inasmuch as in this case there is no exact reference solution available for the displacement field, we have chosen to compute the response first with the TLM+PML and then with a computationally intensive numerical integration over wavenumbers, based on an exact stiffness matrix formulation [18]. Figs 8a,b show the displacement functions for $f = 0.1$ [Hz] and $f = 1$ [Hz]. Once more, the agreement at both frequencies is so close that the response functions obtained by either method can hardly be distinguished from one another. Also, since the other two frequencies gave similarly results, they need not be shown. Thus, the TLM+PML provided virtually exact results.

We mention in passing that additional simulations carried out with a stiffer layer underlain by a soft elastic half-space gave equally spectacular results, but since they are qualitatively similar to those already shown, they can be omitted.

7. PML+TLM for SVP waves

The case of in-plane motions eliciting SVP waves —i.e. both shear and dilatational waves— largely parallels and is qualitatively similar to the previous developments for SH waves. The principal differences in this case are the two distinct speeds of wave propagation in each layer, the duplication in the number of degrees of freedom, and most importantly, the change from a linear eigenvalue in k_j^2 to a more complicated quadratic eigenvalue problem of the form [17]

$$\left(\mathbf{A}k_j^2 + \mathbf{B}k_j + \mathbf{G} - \omega^2\mathbf{M}\right)\boldsymbol{\phi}_j = \mathbf{0} \tag{20}$$

The SVP eigenvalue problem uses once more a set of block-tridiagonal matrices $\mathbf{A},\mathbf{B},\mathbf{G},\mathbf{M}$ and satisfies several orthogonality conditions which are significantly more involved than those of the SH wave problem. Still, although the $\mathbf{A},\mathbf{G},\mathbf{M}$ matrices here are similar to those for SH waves (eq. 15) and show similar dependence on the layer thickness, they are twice as large and depend also on two material parameters in each layer instead of just one, i.e. either the two Lamé constants or the shear modulus and Poisson's ratio. Moreover, the eigenvalue problem includes an additional matrix $\mathbf{B}$ which does not depend on the thickness of the sub-layers, so it is the same in a PML as in a standard layer. Inasmuch as the detailed structure of these matrices and their orthogonality conditions are well known and can be found in earlier works on the TLM [17], they can be omitted. It suffices to add that —as in the SH case— we construct the PML by replacing the actual thicknesses of the layers by their complex, position-dependent values.

As we mentioned in an earlier section on non-physical modes, the quadratic eigenvalue problem is typically solved by iterative methods such as inverse iteration with shift by the Rayleigh quotient, or by a determinant search with deflation of the eigenvalues found. In both of these strategies the iteration can be greatly accelerated by projecting the eigenvalues from one frequency to the next. A straightforward and convenient, yet computationally expensive alternative is to transform the quadratic eigenvalue problem into a non-symmetric, linear eigenvalue problem of double size, and then use standard routines, such as those in Matlab, which can't project eigenvalues. Still, for a moderate number of layers, the computational expense is tolerable —for example, with 200 layers the quadratic eigenvalue problem solved with Matlab in a modern Laptop required only 4 seconds per frequency. However, to avoid numerical problems, it is crucial to check and enforce the orthogonality conditions.

As in the SH case, there exist formulas based on modal superposition —very similar to those in eqs. 18— which allow computing with the TLM the responses to SVP sources placed anywhere in an arbitrarily layered medium [17]. However, unlike the SH case, there are no closed-form canonical solutions available in the frequency domain for any load configuration, not even for a homogeneous half-space subjected to harmonic line loads at its surface (The closed form solution to Lamb's problem is only known in the space-time domain). Thus, verification of half-space problems can only be made against numerical integration over wavenumbers, as already done for the layered SH case. Still, there is one problem for which closed-form results do exist, namely the homogeneous full space: It can be simulated in the TLM by adjoining two PMLs to the elastic layers (EL), one underneath and the other above the layers (or even simpler than that, two adjoined PMLs, an upper and a lower PML). This PML-EL-PML model can in turn be reduced to a EL-PML model of half size by the use of symmetry – antisymmetry considerations for horizontal or vertical loads. This would require modifying appropriately the boundary conditions at the mid-surface of the elastic layer, which constitutes the new free surface of the reduced size model.

As for the optimal parameters for the SVP case, they follow the same rules as for the SH case, provided we choose as reference wavelength the one associated with shear waves, i.e. $\lambda = C_S / f$. This works, because P waves have wavelengths which are about twice as long as those of S waves, and thus are less affected by discretization. For the same reason, however, they may require —at least in principle— a PML which is about twice as deep, yet numerical experiments show that the standard rules work fine up to Poisson's ratios as high as 0.4. We demonstrate the

technique by means of two examples, a full homogeneous space and a layered half-space, namely the same one used earlier as a Love waveguide.

7.1) Example 1: Homogeneous full space

As stated earlier, the homogenous full space subjected to in-plane, horizontal or vertical line loads admits closed form solutions, e.g. [23 p. 38]. This problem is simulated herein with the PML-EL-PML model referred to previously, which can be appropriately reduced to half-size. Assuming unit material properties $G=1$ [Pa], $\rho=1$ [kg/m^3] together with Poisson's ratio $\nu=0.25$, then the wave velocities are $C_S=1$ [m/s] and $C_P=\sqrt{3}$ [m/s]. Although the half-size model alluded to earlier is far more efficient from the computational point of view, here we choose to use the full model for reasons of simplicity. Then again, to make the exercise more interesting, we place the line load with frequency $f=1$ [Hz] in contact with the upper PML and compute the displacements along the interface with the lower PML. We also choose the PML parameters $x_{\max}=20\lambda_S$, $\eta_S=1.4$, $\Omega=4.7$, and $N_{\text{PML}}=14$. The elastic part has a total thickness $H_{\text{EL}}=6\lambda_S$ and is divided into $N_{\text{EL}}=240$ thin-layers, which is far more than needed.

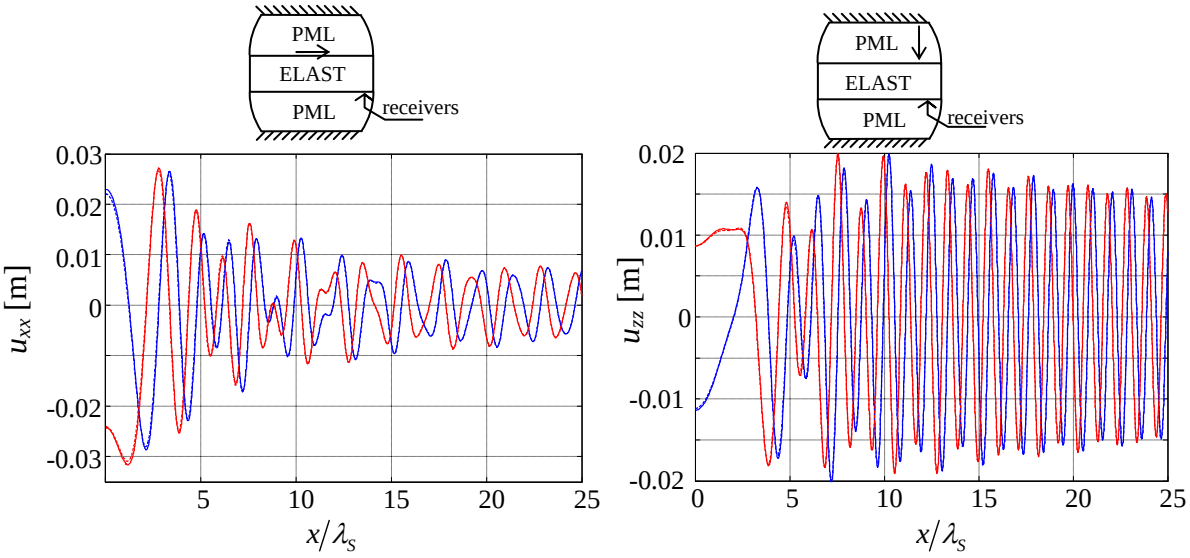

Figure 9 a,b – Real (blue) and imaginary (red) parts of displacements u_{xx} (left) and u_{zz} (right) within a full-space. Solid line = TLM+PML model; Dashed line = exact solution. Differences are virtually nil.

Figs. 9a,b show the horizontal and vertical displacements along the lower PML horizon which are elicited by horizontal and vertical loads, respectively. These figures depict both the TLM+PML solution and also the exact formula for a full space (i.e. the Stokes' formula). The agreement is excellent, with only a slight deviation at small distances, which can be eliminated altogether by moderately increasing the number of thin layers.

7.2) Example 2: Layer over an elastic half-space

We next revisit the Love waveguide of an earlier section but subject it instead to an in-plane, vertical line load placed at the interface of the elastic layers and the PML. We assign to this

system a set of Poisson's ratios $\nu_{\mathrm{EL}} = 0.30$, $\nu_{\mathrm{PML}} = 0.25$ and compute the displacements along the EL-PML horizon.

Figure 10 shows the poles obtained for this problem at four frequencies. As before in the SH case, the dots are for the discrete solution, and the circles are for the exact (continuous) formulation with stiffness matrices and search techniques. Considering that the cutoff frequencies of the layer (for a rigid base condition) are $f_{SV} = C_S / 4H_{\mathrm{EL}} = 0.125$ [Hz], $f_P = f_{SV}\sqrt{3} = 0.217$ [Hz], we see that $f = 0.1$ [Hz] is below both of these, $f = 0.2$ [Hz] is between these two, and both $f = 1$ [Hz] and $f = 10$ [Hz] are well above these reference frequencies. Hence, the first driving frequency can be considered to be "low", the second "intermediate", and the last two to be "high". In contrast to the SH case, we observe that there are now two Bérenger branches.

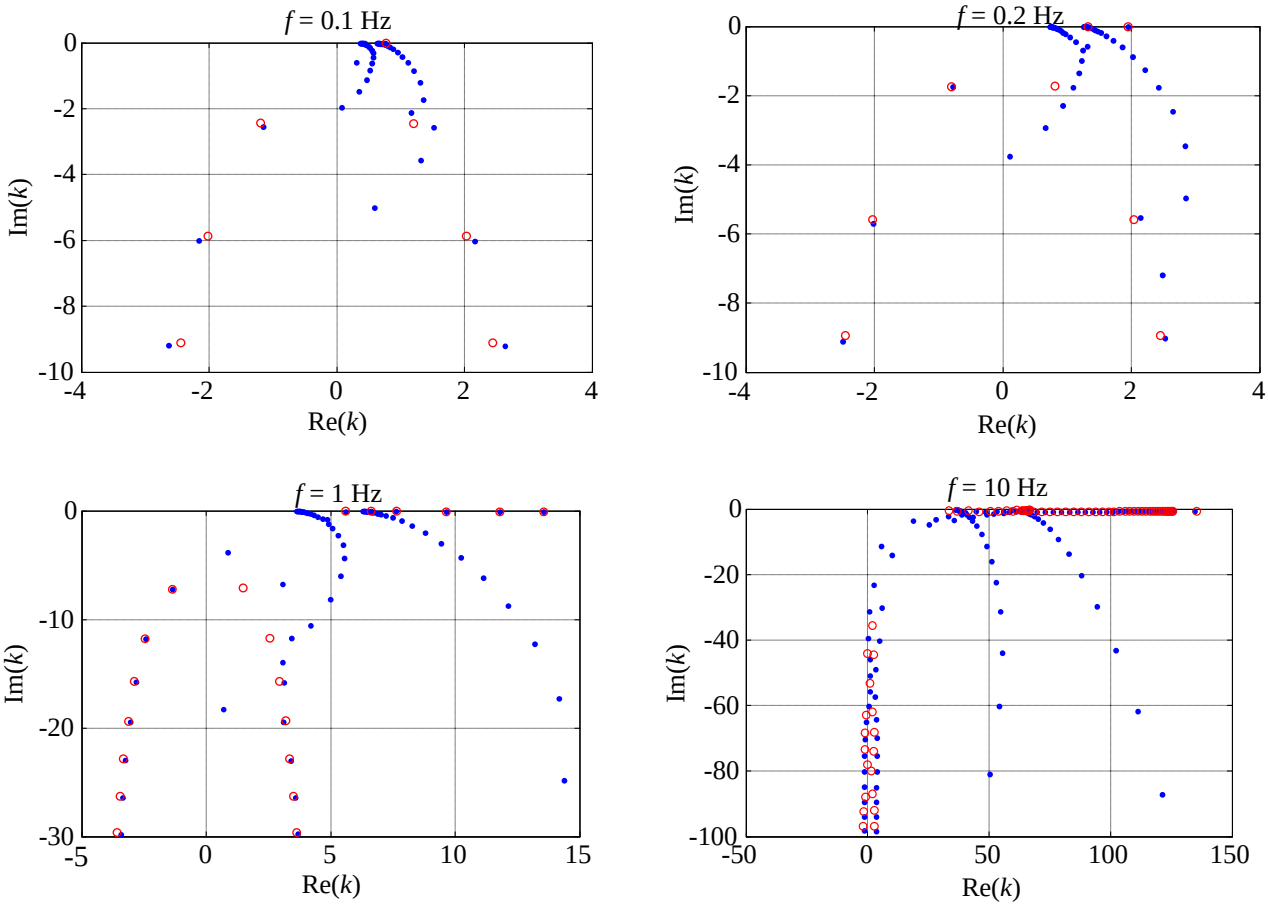

Figure 10 a,b,c,d: Poles of layered system at four frequencies obtained by the TLM+PML (blue dots) and via search techniques (open red circles).

Figure 11 shows two of the four response functions, and compares the TLM+PML solution against a numerical integration over wavenumbers using the exact analytical solution in the frequency-wavenumber domain [18]. The agreement is again excellent, which confirms the quality of the proposed method.

8. PML vs. Paraxial Boundaries (PB)

The standard way to model layered media underlain by infinitely deep elastic half-spaces is by means of paraxial boundaries augmented with buffer layers [14,30,34,35]. Explicit expressions for the PB matrices can be found in e.g. [30, pp. 289], while comments and considerations about their stability can be found in [21,22]. We now go on to compare the performance of the TLM+PML approach against those of the TML+PB approach. For this purpose, we resort once more to the full-space problem for which closed form solutions exist. For the pair of PMLs (i.e. upper and lower), we choose the parameters $\eta = 1.2, \Omega = 4.1$, which we join directly without any intervening elastic layers, while for the PB model, we choose a pair of paraxial boundaries, each of which is augmented with buffer layers which are twice as thick as the PML they substitute for (i.e. $H_{\mathrm{BL}} = 2.4\lambda_S$). These buffer layers are discretized into 24 thin layers each. Both models are subjected to a vertical line load placed on their mid-planes, and vertical displacements are computed at that same elevation and compared against the exact solution.

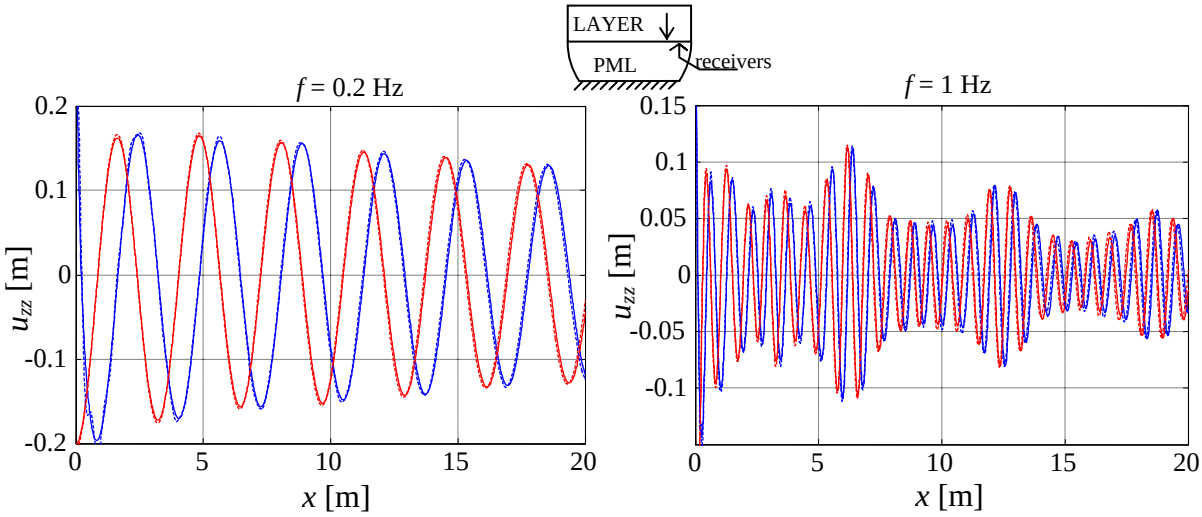

Figure 11 a,b: Real (blue) and imaginary (red) parts of vertical displacements in layered system due to vertical line load at interface of layer and half-space, low and high frequency. Solid line = TLM-PML model; Dashed line = integration over wavenumbers. Differences negligible.

Fig. 12 shows the relative errors of the two approaches, defined as the percent deviation of the absolute values when compared to those of the exact solution. Clearly, the PML approach is substantially more accurate than the PB approach, with errors below 5% up to distances $x = 25\lambda$, while the errors in the second approach exceed 10% even before a distance $x = 5\lambda$, and it becomes intolerable at larger distances. When consideration is also given to the fact that in this example the PML model has only half the number of degrees of freedom of the PB model, it is clear that TLM+PML approach outperforms the TLM+PB approach by a vast margin.

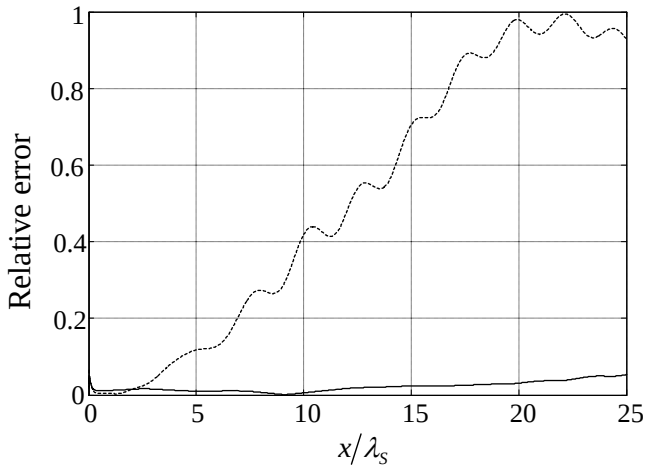

Figure 12 – Relative error: Solid line = TLM+PML; Dotted line = TLM+PB

9. Frequency response functions

Up to this point we have examined the performance of the TLM-PML for problems expressed in terms of a fixed, characteristic wavelength λ. Thus, it behooves now to explain how the preceding material applies to actual engineering examples where the frequency changes over some interval. To illustrate matters, consider a homogeneous elastic half-space with shear wave velocity $C_S = 100$ [m/s] and mass density $\rho = 2000$ [kg/m^3] subjected to an SH line load at the origin on its surface, i.e. $x_s = z_s = 0$. The frequency response functions are desired at receivers placed at $(x_r, z_r) = (50, 0)$ and $(x_r, z_r) = (40, 30)$ meters, i.e. on the surface and at some interior point. Observe that for convenience we choose receivers with identical source-receiver distance, in which case the responses at these two locations should be identical. The load is harmonic with frequencies $f = 0.1:0.1:10$ [Hz] at 0.1 [Hz] intervals. The exact solution is given by equation (11) (with $r_1 = r_2 = 50$ [m]), while the TLM-PML solution can be found by constructing a model consisting of an upper elastic part that is as deep as the deepest receiver $H_1 = 30$ [m], coupled to a PML with the same material properties as the elastic part, and parameters to be decided.

At 10 [Hz] the characteristic wavelength in both the layer and the PML is $\lambda = C_S / f = 10$ [m], which is the shortest wavelength. Choosing 20 thin layers per wavelength, this gives a total of $20 H_1 / \lambda = 20 \times 30 / 10 = 60$ thin layers for the elastic part. Although at lower frequencies one could get away with fewer thin layers, this is really not necessary, for the number for layers is not excessive, and keeping it constant allows assembling the layer matrices $\mathbf{A}_{\mathrm{EL}}, \mathbf{G}_{\mathrm{EL}}, \mathbf{M}_{\mathrm{EL}}$ for the elastic part once and for all without further adjustments. Besides, the accuracy at close range where strain gradients are high depends also on the refinement of the model, and not just on the frequency.

As for the PML and from eqs. 19, we choose $x_{\max} = 100$ [m] (twice the maximum range of interest), which gives

$$\eta = \frac{H_2}{\lambda} = \sqrt[3]{\tfrac{1}{12} x_{\max} f / C_S} = \sqrt[3]{\tfrac{1}{12} 100/100 \times f} = \sqrt[3]{\tfrac{1}{12} f} = \begin{cases} 0.20 & f = 0.1 \text{ [Hz]} \\ 0.94 & f = 10 \text{ [Hz]} \end{cases}$$

which means that $\eta = 1$ and $\Omega = 4\eta = 4$ will satisfy all frequencies, so $H_2 = \lambda = C_S / f = 100 / f$. Hence, the depth of the PML decreases with the frequency from $H_2 = 1000$ [m] at $f = 0.1$ [Hz] to $H_2 = 10$ m at $f = 10$ [Hz]. Using linear elements, i.e. $n = 1$, the number of layers in the PML is then $N = 10\eta / n = 10$. Inasmuch as this number does not change with frequency, the element thickness appears explicitly in the layer matrices, and the imaginary part depends only on the dimensionless ratio $\zeta = z / H$ within the element, it is possible to construct and assemble the layer matrices for the PML a priori with $H_2 = 1$ [m], and thence multiply the $\mathbf{A}_{\text{PML}}, \mathbf{M}_{\text{PML}}$ matrices and divide the $\mathbf{G}_{\text{PML}}$ matrix by the actual H_2 at the current frequency. Thereafter, one simply superposes the layer matrices for the elastic part and the PML, which gives the system matrices at the current frequency. One then solves the eigenvalue problem at the current frequency and proceeds to find the displacements at the receivers by means of eq. 18. Needless to add, in the case of a half-space with different properties from the elastic layer, one would have to use the respective wavelengths in the layer and in the half-space to determine the parameters for each of the two parts.

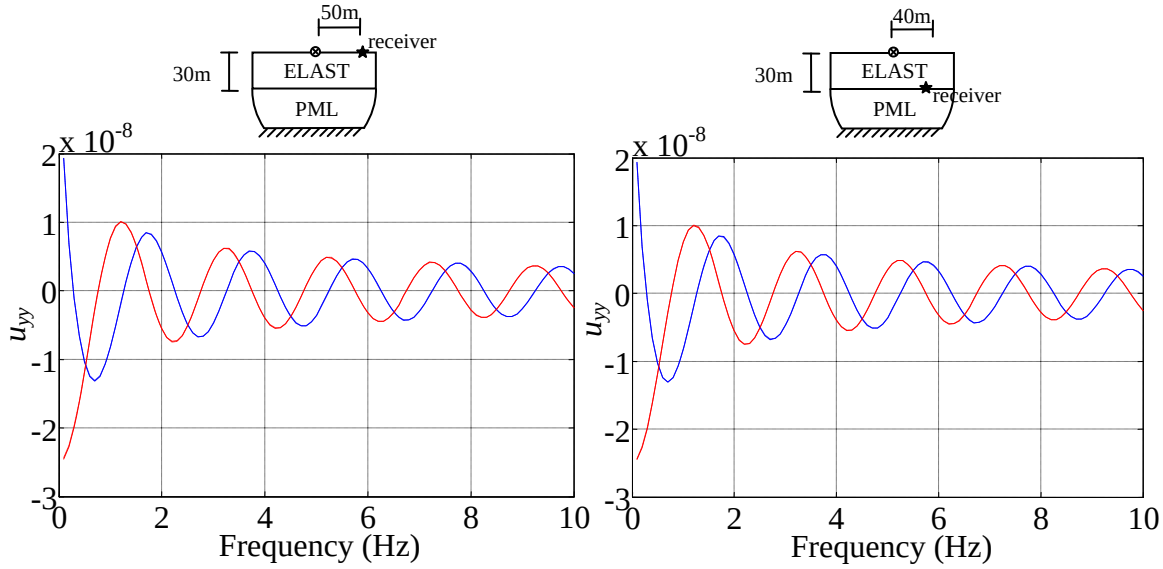

Figure 13a,b– Real (blue) and imaginary (red) parts of u_{yy} displacements for positions (0, 50) [m] (left) and (40, 30) [m] (right): Dashed and solid lines are the PML approximation and exact solutions, respectively. Differences are undetectable, even at larger scale.

Fig. 13a,b shows the displacements as function of frequency for receivers at the positions (50, 0) m and (40, 30) m, calculated by the TLM+PML and by the exact expression (11). No differences can be seen between the two approaches, as expected. Also, the figures are exactly the same, as explained by the fact that the two receivers are at the same distance from the source.

10. Conclusions

This article demonstrated the use of the Perfectly Matched Layer (PML) concept in the context of the Thin Layer Method (TLM) for both anti-plane (SH) and in-plane (SVP) models, and by implied extension, to layered systems formulated in cylindrical coordinates (i.e. point loads, ring load, disk loads and so forth). It was shown that this approach results in spectacularly accurate results which hardly differ from analytical formulas for known canonical problems. Moreover, the results are vastly superior to those of the conventional approach which relies on paraxial boundaries, and accomplishes this improvement with fewer degrees of freedom. Thus, this approach is likely to become the method of choice for this class of problems. Nonetheless, that will probably occur only after the current algorithms for the quadratic eigenvalue problem based on inverse iteration are made reliably robust and freed from numerical difficulties associated with some modes. This would allow projecting eigenvalues from one frequency to the next while taking full advantage of the block-tridiagonal structure of the TLM matrices, both of which exert an enormous influence on the computational efficiency. The writers are now addressing this interesting problem.

Acknowledgement

The first author wishes to thank the financial support he received from the *Fundação para a Ciência e a Tecnologia* of Portugal (FCT) through grant number SFRH/BD/47724/2008 and from the *Risk Assessment and Management for High-Speed Rail Systems*' project of the MIT—Portugal Program in the Transportation Systems Area. He also wishes to thank his academic advisors Prof. Rui Calçada and Prof. Álvaro Azevedo of the University of Oporto for arranging his traineeship at MIT as a visiting student under the umbrella of the MIT-Portugal Program.

Appendix A: Convergence of modal summation for SH loads

a) Continuous model

As mentioned earlier in this article, the modal solution at interior points in the PML may break down because the stretched, complex coordinates appear as arguments in trigonometric functions. This gives rise to hyperbolic terms within the PML which not only may elicit severe cancellation errors , but which may cause the modal superposition to fail to converge —but observe that this is only a problem for the modal expansion formula, for the PML itself still performs as expected. We examine this problem in some detail herein.

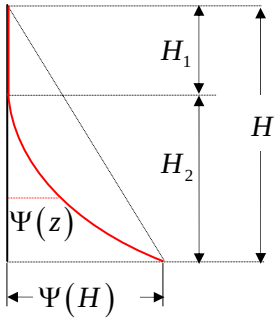

Figure 14: Variation of stretching function

Consider a uniform stratum of depth H subjected to anti-plane SH waves, which is converted into a generalized PML by an appropriate stretching function $\Psi(z)$ which satisfies eqs. 1,2 . In principle the stretching function is arbitrary —as long as it is non-negative and grows monotonically with z . Thus, we can choose to subdivide the system into an upper *elastic* part of thickness H_1, and a lower part of thickness H_2 which obeys the stretching function 3, appropriately shifted to begin at the interface between these two parts. Thus, the stretching function is as shown schematically in Fig. 14. It follows that

$$\Psi(z)=\begin{cases} 0 & z\le H_1 \\ \Omega H_2\left(\dfrac{z-H_1}{H_2}\right)^{m+1} & H_1\le z\le H \end{cases} \tag{A1a}$$

$$\bar{z}=z-\mathrm{i}\,\Psi(z) \tag{A1b}$$

In stretched space, the stratum is still "homogeneous", so the exact modal solution of this system continues to be given by eqs. 12, which for convenience we repeat below in a slightly modified, dimensionless form:

$$\kappa_j=k_jH\,,\qquad \xi=\frac{|x|}{H},\qquad a_0=\frac{\omega H}{C_S},\qquad \bar{\zeta}=\frac{\bar{z}}{\bar{H}},\qquad \theta_j=\pi\left(j-\tfrac{1}{2}\right) \tag{A2a}$$

$$u_{yy}(x,\omega)=\frac{1}{\mathrm{i}G}\sum_{j=1}^{\infty}\phi_j(\bar{z}_s)\phi_j(\bar{z}_r)\frac{\mathrm{e}^{-\mathrm{i}\kappa_j\xi}}{k_j\bar{H}} \tag{A2b}$$

$$\kappa_j=\sqrt{a_0^2-\left(\frac{H}{\bar{H}}\right)^2\theta_j^2} \tag{A2c}$$

$$\phi_j(\bar{z})=\cos\left(\theta_j\bar{\zeta}\right) \tag{A2d}$$

We observe that the precise variation of the stretching function $\Psi(z)$ within the system only affects the eigenvectors (eq. A2d), while the eigenvalues (eq. A2c) depend solely on the total complex depth $\bar{H}$. Next, we proceed to express the various complex quantities in terms of their real and imaginary parts, and write the complex depth $\bar{z}$ and total thickness $\bar{H}$ of the stratum as

$$\bar{z}=z_R-\mathrm{i}\,z_I \tag{A3a}$$

$$\bar{H}=H_R-\mathrm{i}\,H_I\,,\qquad H_R\equiv H=H_1+H_2\,,\qquad H_I\equiv\Omega H_2 \tag{A3b}$$

Hence,

$$\bar{\zeta}=\frac{\bar{z}}{\bar{H}}=\frac{z_R-\mathrm{i}\,z_I}{H_R-\mathrm{i}\,H_I}=\frac{(z_R-\mathrm{i}\,z_I)(H_R+\mathrm{i}\,H_I)}{H_R^2+H_I^2}=\frac{(z_RH_R+z_IH_I)+\mathrm{i}\,(z_RH_I-z_IH_R)}{H_R^2+H_I^2}=A+\mathrm{i}\,B \tag{A4a}$$

with

$$A = \frac{z_R H_R + z_I H_I}{H_R^2 + H_I^2} \qquad B = \frac{z_R H_I - z_I H_R}{H_R^2 + H_I^2} \tag{A4b}$$

Also, for large values of the modal counter j, the eigenvalue tends asymptotically to

$$\kappa_j \to -\mathrm{i}\frac{H}{\bar{H}}\theta_j = -\mathrm{i}\frac{H_R}{H_R - \mathrm{i}H_I}\theta_j = \frac{H_R\left(H_I - \mathrm{i}H_R\right)}{H_R^2 + H_I^2}\theta_j \tag{A5}$$

so

$$\begin{aligned} \mathrm{e}^{-\mathrm{i}\kappa_j\xi} &\to \exp\left(-\mathrm{i}\frac{H_R\left(H_I - \mathrm{i}H_R\right)}{H_R^2 + H_I^2}\theta_j\xi\right) \\ &= \exp\left(-\frac{H_R^2\xi}{H_R^2 + H_I^2}\theta_j\right)\exp\left(-\mathrm{i}\frac{H_R H_I\xi}{H_R^2 + H_I^2}\theta_j\right) \sim \exp\left(-C\theta_j\right) \end{aligned} \tag{A6}$$

where

$$C = \frac{H_R^2\xi}{H_R^2 + H_I^2} = \frac{H_R|x|}{H_R^2 + H_I^2} \tag{A7}$$

Also

$$\begin{aligned} \cos\theta_j\bar{\zeta} &= \cos\left(A\theta_j + \mathrm{i}B\theta_j\right) = \cos A\theta_j \cosh B\theta_j - \mathrm{i}\sin A\theta_j \sinh B\theta_j \\ &= \tfrac{1}{2}\left[\exp\left(B\theta_j\right)\exp\left(-\mathrm{i}A\theta_j\right) + \exp\left(-B\theta_j\right)\exp\left(\mathrm{i}A\theta_j\right)\right] \end{aligned} \tag{A8}$$

Now, B can be either positive or negative, but whatever the sign, one of the two exponential terms above will grow with $\theta_j \sim \pi j$, so the j^{th} modal shape is of order $\cos\theta_j\bar{\zeta} \sim \exp\left(|B|\theta_j\right)$. Adding subscripts s, r to identify to the locations of the source and the receiver, respectively, it follows that the modal summation will include terms of order

$$\cos\theta_j\bar{\zeta}_s \cos\theta_j\bar{\zeta}_r \mathrm{e}^{-\mathrm{i}\kappa_j\xi} \sim \exp\left(|B_s|\theta_j\right)\exp\left(|B_r|\theta_j\right)\exp\left(-C\theta_j\right) = \exp\left[\left(|B_s| + |B_r| - C\right)\theta_j\right] \tag{A9}$$

It can be seen from eq. A9 that for the modal summation to converge, it is necessary that

$$C > |B_s| + |B_r| \quad \to \quad \frac{H_R|x|}{H_R^2 + H_I^2} > \frac{\left|z_{Rs}H_I - z_{Is}H_R\right|}{H_R^2 + H_I^2} + \frac{\left|z_{Rr}H_I - z_{Ir}H_R\right|}{H_R^2 + H_I^2} \tag{A10}$$

i.e.

$$\boxed{|x| > \frac{\left|z_{Rs}H_I - z_{Is}H_R\right| + \left|z_{Rr}H_I - z_{Ir}H_R\right|}{H_R}} \tag{A11}$$

If the source and receiver are both in the upper elastic section, then $z_{Rs} \equiv z_s, z_{Rr} \equiv z_r$, $z_{Is} = z_{Ir} = 0$, in which case

$$|x| > \frac{H_I}{H_R}\left(z_s + z_r\right) \equiv \Omega\frac{H_2}{H}\left(z_s + z_r\right), \qquad 0 \le z_s, z_r \le H_1, \qquad H = H_1 + H_2 \tag{A12}$$

This implies that when the source and receiver are both at the surface, the continuous series converges for all $|x|$, yet that is not the case if either the source or the receiver is within the elastic region. On the other hand, when both the source and receiver are within the PML, then

$$|x| > \Omega H_2 \left\{ \left| \frac{z_s}{H} - \left(\frac{z_s - H_1}{H_2} \right)^{m+1} \right| + \left| \frac{z_r}{H} - \left(\frac{z_r - H_1}{H_2} \right)^{m+1} \right| \right\} \tag{A13}$$

In the case of a pure PML, i.e. $H_1 = 0$, $H_2 = H$, then

$$|x| > \Omega H \left\{ \frac{z_s}{H} \left(1 - \left(\frac{z_s}{H} \right)^m \right) + \frac{z_r}{H} \left(1 - \left(\frac{z_r}{H} \right)^m \right) \right\} \tag{A14}$$

In summary, we have shown that —except at the surface— the modal summation for the continuous medium does not converge at close ranges, which at first would seem disappointing. Fortunately, the TLM implementation of the PML does indeed converge everywhere within the elastic part, as was already clearly demonstrated in the main text, and taken up again in the next section.

b) Discrete model

It would appear from the preceding that use of the PML method as boundary condition for a TLM model is doomed to fail at close range, and thus render the proposed method unattractive, but this is fortunately not the case. As it turns out, the discrete PML behaves in an intrinsically different way from the continuous PML, even when a very large number of thin layers is used in the discretization. The differences lie in both the eigenvalues (i.e. poles) and the eigenvectors.

Consider a single PML for SH waves (i.e. with no elastic part) of unit depth and subjected to excitations of unit wavelength. If we divide this medium into $N = 1000$ thin layers, each one is but a tiny fraction of either the thickness or the characteristic wavelength. Extrapolating from experience with finite elements, one might surmise that at least half of the eigenvalues of such a TLM model will be close to those of the continuous medium, but that is in fact not the case. Instead, the discretization causes massive changes in the pole spectrum, as demonstrated in Figure 15.

This figure shows the first thousand of the infinitely many poles for the continuum solution as stars, which begin at the branch point $k_0 = \omega / C_S = 2\pi$ on the real axis, and continue along a nearly straight line into the complex k domain; also shown as circles are the thousand discrete poles. Although a small subset of the discrete modes follows closely the continuous solution at first —about fifty modes or 5%— thereafter the TLM poles are scattered over a broad area surrounded by well defined boundaries. Most TLM poles (95%) have very large imaginary parts, and are thus highly evanescent —indeed, much more so than the continuous poles. At the same time, the eigenvectors also experience correspondingly large changes once the eigenvalues begin to disagree.

So why does the TLM then converge? In a nutshell, the discrete system converges not only because the modal summation extends over a finite number of modes, but also because most

TLM+PML poles are highly evanescent and thus they contribute virtually nothing to the response A similar phenomenon is observed when the PML is overlain by elastic layers.

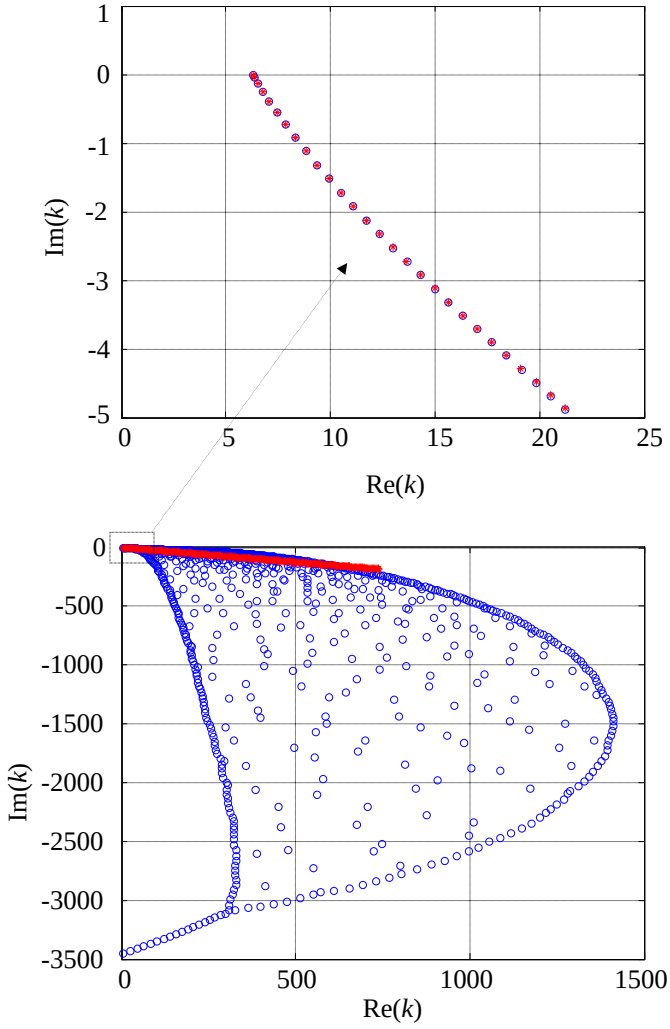

Figure 15 a,b: Continuous vs. discrete poles of PML system for SH waves. TLM model consists of N=1000 layers. The close-up above shows the first thirty or so modes, which agree perfectly.

In principle, if one were to subdivide the PML into an obscene number of thin layers, that system would begin exhibiting some of the problems of the continuous solution. However, this is never necessary. The discretization of the PML is controlled by the optimal parameters given earlier in the text, and there is absolutely no need to increase this number even further. Clearly, such course of action does not preclude the option of choosing many thin layers for the *elastic* part, should the driving frequency demand such thin layers. Still, one should evaluate displacements only in the elastic part, and abstain from computing them within the discrete PML, for they have no useful meaning.

References

1. Alsop, L.E. (1970): "The leaky-mode period equation—a plane wave approach", *Bulletin of the Seismological Society of America*, **60** (6): 1989-1998.
2. Alsop, L.E., Goodman, A.S., and Gregersen, S. (1974): "Reflection and transmission of inhomogeneous waves with particular application to Rayleigh waves", *Bulletin of the Seismological Society of America*, **64** (6): 1635-1652.
3. Basu, U. and Chopra, A.K. (2004): "Perfectly matched layers for transient elastodynamics of unbounded domains", *International Journal for Numerical Methods in Engineering*, **59**:1039-1074.
4. Bérenger, JP (1994): "A perfectly matched layer for the absorption of electromagnetic waves", *Journal of Computational Physics*, **114** (2): 185-200.
5. Bienstman, P., Olyslager, F., (2001), "Analysis of cylindrical waveguide discontinuities using vectorial eigenmodes and perfectly matched layers", *IEEE Transactions on Microwave Theory and Techniques*, **49** (2): 349-354.
6. Bienstman, P., Baets, R. (2002): "Advanced boundary conditions for eigenmode expansion models", *Optical and Quantum Electronics*, **34**, 523-540.
7. Bougacha, S., Tassoulas, J. and Roësset, J. (1993): "Analysis of foundations on fluid-filled poroelastic stratum", *Journal of Engineering Mechanics*, **119** (8): 1632-1648.
8. Chakraborty, A., Gopalakrishnan, S ., and Kausel, E. (2005):"Wave propagation analysis in inhomogeneous piezo-composite layer by the thin-layer method", *International Journal for Numerical Methods in Engineering*, **64**: 567-598.
9. Chew, W., Liu, Q. (1996): "Perfectly matched layers for elastodynamics: A new absorbing boundary condition", *Journal of Computational Acoustics*, **4 (4)**: 341-359.
10. Collino, F. and Tsogka, Ch. (2001): Application of the perfectly matched absorbing layer model to the linear elastodynamic problem in anisotropic heterogeneous media", *Geophysics*, **66** (1):294-307.
11. Derudder, H., Olyslager, F. (2001): "Efficient mode-matching analysis of discontinuities in finite planar substrates using perfectly matched layers", *IEEE Transactions on Antenas and Propagation*, **49** (2): 185-195.
12. Ghibril, R. (1992): "On the partial discretization of coupled plane stratified systems", *PhD Thesis*, Department of Civil and Environmental Engineering, MIT, Cambridge, Massachusetts
13. Harari, I., Albocher, U. (2006): "Studies of FE/PML for exterior problems of time-harmonic elastic waves", *Computer Methods in Applied Mechanics and Engineering*, **195**: 3854-3879.
14. Hull [Seale], S. and Kausel, E. (1984): "Dynamic loads in layered halfspaces", *Proceedings, Fifth Engineering Mechanics Division Specialty Conference*, ASCE, I, 201-204, Laramie, Wyoming, August 1984.
15. Joanni, A. E., and Kausel, E. (2009): "Heat diffusion in layered media via the thin-layer method", *International Journal for Numerical Methods in Engineering*, **78** (6): 692-712.
16. Johnson, S. G. (2010): "Notes on Perfectly Matched Layers", Lecture notes, Department of Mathematics, Massachusetts Institute of Technology, downloadable from: http://math.mit.edu/~stevenj/18.369/pml.pdf
17. Kausel, E. (1981): "An explicit solution for the Green's functions for dynamic loads in layered media", *MIT Research Report R81-13*, Department of Civil Engineering, MIT, Cambridge, MA 02139.
18. Kausel, E., Roësset, J. (1981): "Stiffness matrices for layered soil", *Bulletin of the Seismological Society of America*, **71**: 1743-1761.
19. Kausel, E. and Peek, R. (1982): "Dynamic loads in the interior of a layered stratum: An explicit solution", *Bull. Seism. Soc. Am.*, **72** (5): 1459-1481 (see also Errata in *BSSA*, **74** (4), 1984. p. 1508).
20. Kausel, E. (1986): "Wave Propagation in Anisotropic Layered Media", *International Journal for Numerical Methods in Engineering*, **23**: 1567-1578.
21. Kausel, E. (1988): "Local Transmitting Boundaries", *Journal of Engineering Mechanics*, ASCE, **114** (6):1011-1027.
22. Kausel, E. (1992): "Physical interpretation and stability of paraxial boundary conditions", *Bulletin of the Seismological Society of America*, **82**(2): 898-913.
23. Kausel, E. (2006): *Fundamental Solutions in Elastodynamics: A Compendium*, Cambridge University Press, Cambridge, UK. See also the brief *Corrigendum* together with an extensive *Addendum* at the following Internet address: "http://www.mit.edu/afs/athena.mit.edu/user/k/a/kausel/Public/webroot/articles/Green Functions/Fundamental Solutions, Corrigendum.pdf

24. Kausel, E. and Barbosa, J. (2010): "PMLs: A direct approach", *International Journal for Numerical Methods in Engineering*, published online in Wiley Online Library (wileyonlinelibrary.com). DOI: 10.1002/nme.3322.
25. Kucukcoban, S., Kallivokas, L.F. (2010): "Mixed perfectly-matched-layers for direct transient analysis in 2D elastic heterogeneous media", *Computer Methods in Applied Mechanics and Engineering*, **200** (1-4): 57-76.
26. Lotfi, V., Roësset, J. M. and Tassoulas, J. L. (1987): "A technique for the analysis of the response of dams to earthquakes", *Earthquake Engineering & Structural Dynamics*, **15**: 463–489.
27. Lysmer, J. (1970): "Lumped mass method for Rayleigh waves", *Bulletin of the Seismological Society of America*, **60**(1): 89-104.
28. Lysmer, J. and Waas, G. (1972): "Shear waves in plane infinite structures", *Journal of the Engineering Mechanics Division*, **98**(1): 85-105.
29. Park, J. (1998): "Point sources in cylindrically laminated rods", *S.M Thesis*, Department of Civil and Environmental Engineering, MIT, Cambridge, Massachusetts.
30. Park, J. (2002): "Wave motion in finite and infinite media using the Thin-Layer Method", *PhD Thesis*, Department of Civil and Environmental Engineering, MIT, Cambridge, Massachusetts.
31. Park, J and Kausel, E. (2004): "Numerical dispersion in the thin-layer method", *Computers and Structures*, **82**: 607-625.
32. Rogier, H., Zutter, D. (2001): "Berenger and leaky modes in microstrip substrates terminated by a perfectly matched layer", *IEEE Transactions on Microwave Theory and Techniques*, **49**(4): 712-715.
33. Schlue, J. W. (1979): "Finite element matrices for seismic surface waves in three-dimensional structures", *Bulletin of the Seismological Society of America*, **69**(4): 1425-1438.
34. Seale, S. (1985): "Dynamic loads in layered halfspaces", *PhD Thesis*, Department of Civil and Environmental Engineering, MIT, Cambridge, Massachusetts.
35. Seale, S. and Kausel, E. (1989): "Point loads in cross-anisotropic layered halfspaces", *Journal of Engineering Mechanics*, **115** (3): 509-542.
36. Tan, H. H. (1989): "Displacement approach for generalized Rayleigh waves in layered solid-fluid media", *Bulletin of the Seismological Society of America*, **79** (4): 1251-1263.
37. Tassoulas, J.L. and Kausel, E. (1983): "Elements for the Numerical Analysis of Wave Motion in Layered Strata", *Int. J. Num. Meth. Eng.*, **19**: 1005-1032.
38. Tassoulas, J.L. and Kausel, E. (1983): "On the Dynamic Stiffness of Circular Ring Footings on an Elastic Stratum", *Int. J. Num. Anal. Meth. Geomech.*, **8**: 411-426.
39. Tsai, C., Lee, G. and Ketter, R. (1990): "A semi-analytical method for time-domain analyses of dam-reservoir interactions", *International Journal for Numerical Methods in Engineering*, **29** (5): 913-933.
40. Wolf, J. P. (2003): *The Scaled Boundary Finite Element Method*, Wiley, England
41. Waas, G. (1972): "Linear two-dimensional analysis of soil dynamics problems in semi-infinite layered media", *PhD Thesis*, University of California, Berkeley.
42. Zheng, Y. and Huang, X., (2002): "Anisotropic perfectly matched layers for elastic waves in Cartesian and curvilinear coordinates", *Earth Resources Laboratory 2002 Industry Consortium Meeting*, Dept. of Earth, Atmospheric, and Planetary Sciences, Massachusetts Institute of Technology (MIT).